

Optimizing Structural, Optical, Photocatalytic Properties of Cadmium Substituted Al Nano Chromites Synthesized at Low Temperature

CH. SRIKANTH¹, P. SAILAJA KUMARI¹, R. VENKATESH NAYAK¹ and G. VIJAYA CHARAN^{1*}

Department of Chemistry, University College of Science, Osmania University, Hyderabad-500007, India

*Corresponding author: E-mail: drvijayacharan@gmail.com

Received: 27 December 2024;

Accepted: 18 February 2025;

Published online: 28 February 2025;

AJC-21931

In this work, the fabrication of cadmium doped Al nano chromites was performed by citrate gel auto combustion method to optimize its structural, morphological, optical and photocatalytic properties. The formed cadmium doped Al nanostructured chromites [Al_{1-x}Cd_xCr₂O₄ where $x = 0.00, 0.04$ and 0.10] were characterized by X-ray diffraction, FESEM and FTIR techniques. The XRD confirms the single-phase cubic spinel structure of the Cd-Al nanochromites. The average crystalline size of the samples varies from 19 nm to 25 nm calculated by Debye-Scherrer's equation from X-ray diffraction pattern. FTIR spectrum confirm the metal oxygen bonds around 400 to 600 cm⁻¹ related to the spinel structure. The optical band gap energy ranges from 2.21 eV to 2.90 eV as calculated by Tauc plots. The photocatalytic degradation of methylene blue and acid red dyes under visible light irradiation were performed.

Keywords: Nano chromites, Cadmium doping, Optical properties, Dye degradation.

INTRODUCTION

Nanomaterials are advanced materials with dimensions at the nanoscale, offering unique properties that differ significantly from their bulk counterparts [1,2]. They can be broadly categorized into carbon-based materials (e.g. graphene and carbon nanotubes), metal and metal oxide nanoparticles (e.g., Ag, TiO₂, ZnO, etc.), ceramic nanomaterials, polymeric nanomaterials, nanocomposites, etc. [3-5]. Among these, nano chromites, spinel-structured nanomaterials (AB₂O₄), hold particular importance for their multifunctional properties. Nanochromites like NiCr₂O₄ and CuCr₂O₄ exhibit excellent catalytic activity, magnetic properties and thermal stability, making them suitable for applications in pollutant degradation, energy storage, sensors and magnetic storage devices [6,7].

Cadmium doped Al nano chromites are the class of spinel-structured materials and belong to the family of mixed-metal oxides where cadmium (Cd) and aluminium (Al) occupy specific lattice positions, forming a cubic spinel structure with unique physical and chemical properties. The structure consists of a cubic close-packed oxygen lattice with cations occupying interstitial tetrahedral and octahedral sites. In normal spinels like CdCr₂O₄, Cd²⁺ ions predominantly occupy the tetrahedral sites,

while Al³⁺ ions occupy the octahedral sites [8,9]. This arrangement ensures charge neutrality and structural stability.

Nanoparticles can be synthesized using various methods, each tailored to achieve specific properties and applications. Chemical methods such as sol-gel processing [10], polyacrylamide method [11], microemulsion, co-precipitation, solid state and hydrothermal methods [12], offer versatility in producing nanoparticles with controlled size and morphology. Among these, the citrate gel auto-combustion method stands out due to its simplicity, cost-effectiveness and ability to produce highly pure, homogeneously sized nanoparticles [13]. This method involves the use of metal nitrates and citric acid to form a gel, which undergoes self-sustained combustion to yield fine particles. Particularly effective for synthesizing spinel structured materials like nano chromites, this method ensures phase purity, uniformity and scalability, making it invaluable for applications in catalysis, energy storage and environmental remediation [14].

Among the hazardous dyes, methylene blue, a water-soluble dye, can cause hypoxia in aquatic ecosystems and irritation in humans [15], whereas acid red dye contributes to water pollution by reducing light penetration and disturbing aquatic life [16]. Such pollutants demand urgent attention, requiring effec-

tive treatment technologies such as photocatalysis, adsorption and advanced oxidation processes to prevent long-term environmental damage. Photocatalytic activity is of immense importance in addressing global environmental and energy challenges due to its ability to harness light energy to drive chemical reactions [17]. In current study, the fabrication of cadmium doped Al nano chromites ($\text{Al}_{1-x}\text{Cd}_x\text{Cr}_2\text{O}_4$ where $x = 0.00, 0.04$ and 0.10) was achieved by citrate gel auto combustion method. The prepared samples were characterized by XRD, SEM and FTIR techniques. The study investigates the impact of cadmium doped Al nano chromites for its structural, optical and photocatalytic activities.

EXPERIMENTAL

The cadmium-doped Al nanochromites were synthesized using the citrate gel auto-combustion method with controlled composition and morphology. The synthesis begins with the dissolution of different stoichiometric amounts of aluminium nitrate, cadmium nitrate and chromium nitrate in deionized water to prepare a clear solution. Citric acid was then added in a 1:3 molar ratio acting as a chelating agent and fuel. The citric acid forms stable complexes with the metal ions, ensuring uniform distribution. Ammonia solution was added dropwise to adjust the pH to a range of 7-8. The solution was heated on a hot plate at approximately 80-90 °C with continuous stirring to reduce the water content, till the solution becomes viscous and eventually transforms into a gel. The temperature was then increased to 150 °C, where the gel undergoes a spontaneous combustion reaction. A porous, fluffy, ash-like cadmium-doped Al nanochromite was obtained and then calcined at 500 °C for 4 h in a muffle furnace. The calcined powder was grinded for 1 h to obtain fine powder.

Characterization: A Rigaku 600 X-ray diffractometer was used for the X-ray diffraction investigation. The Carl Zeiss Ultra 55 model was used for SEM analysis and the Oxford INCAx-act model handled EDX analysis. The Fluoromax Plus spectrometer was utilized for photoluminescence (PL) in the range of 350–700 cm^{-1} . The FTIR analysis was conducted in the range of 4000–400 cm^{-1} using Shimadzu FTIR 8400 spectrometer. The optical properties were studied with the help of Shimadzu UV-3600 spectrometer in the wavelength range of 200-700 nm.

RESULTS AND DISCUSSION

X-Ray diffraction studies: Chromites, which often exhibit spinel structures, have distinct diffraction patterns that help confirm phase purity. The X-ray diffraction patterns of cadmium doped Al nano chromites synthesized by citrate gel auto combustion method. Fig. 1 shows the distinct peaks corresponding to crystalline phases, providing insights into the structural and compositional nature of these materials. The consistent peak positions among all samples suggest that the primary structure is shared, while variations in the peak intensity and sharpness indicate differences in crystallinity, phase purity or microstructural properties. The observed peaks are characteristic of a spinel structure, which is typical for chromite-based materials. The spinel phase crystallizes in the cubic system with the space group

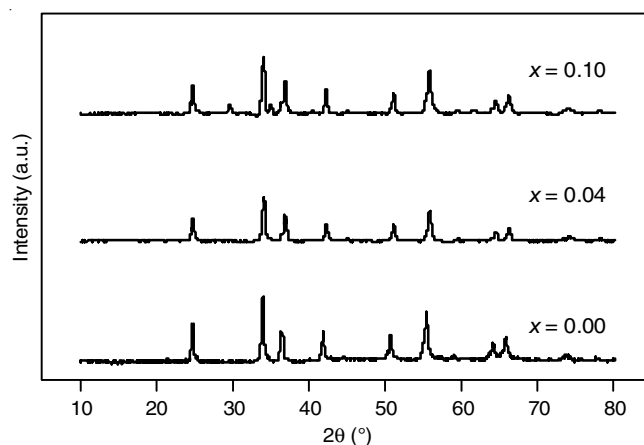


Fig. 1. XRD patterns of $\text{Al}_{1-x}\text{Cd}_x\text{Cr}_2\text{O}_4$ where $x = 0.00, 0.04$ and 0.10

$Fd\bar{3}m$, where metal ions occupy tetrahedral and octahedral positions in the oxygen framework [18,19]. Peaks at low 2θ 19°, 30° and 36°, correspond to the (111), (220) and (311) planes, respectively [20]. Slight shifts in the peak positions among the patterns can be attributed to variations in the Cd and Al composition, as the substitution of larger Cd ions affects the lattice parameters. While the spinel phase dominates as some patterns exhibit additional peaks or changes in peak shapes indicating the possible presence of secondary phases. These could include FCC-type structures, such as Cd-O, which might form due to the segregation of Cd under synthetic conditions [21].

The average crystalline size of the samples calculated by using Debye-Scherrer equation:

$$\text{Average crystalline size (d)} = \frac{0.94\lambda}{\beta \cos \theta}$$

where λ is the wavelength, β is the full width half maxima and θ is the Bragg's angle. The crystalline size of cadmium doped Al nanochromites exhibits a different pattern as the amount of cadmium in the spinal material increases. Crystalline size increases initially at the composition of 0.04, which is attributed due to cadmium ions in the Al_2O_3 matrix facilitating grain development. During this phase, doping of Cd reduces lattice strain, allowing for more ordered and larger crystal formation. However, beyond the peak, the crystalline size starts to decrease slightly and stabilizes at higher Cd compositions. This reduction led due to the formation of lattice defects, such as vacancies and dislocations, as caused by the excessive doping of Cd ions, which disrupts the crystalline order and limits further growth. Lattice parameter of the samples was calculated by the following equation:

$$\text{Lattice parameter (a)} = d\sqrt{h^2 + k^2 + l^2}$$

whereas d is the interplanar distance and hkl indicates the miller indices. The lattice parameter of Cd-doped Al decreases consistently with increasing Cd composition. This trend is primarily due to the ionic radius difference between Al^{3+} (0.53 Å) and Cd^{2+} (0.95 Å). When larger Cd^{2+} ions replace smaller Al^{3+} ions in the lattice, the overall structure experiences a reduction as it adjusts to accommodate the substitution. This decrease in

the lattice parameter suggests a systematic and homogeneous incorporation of Cd ions into the AlCr_2O_4 matrix. The observed behaviour aligns with Vegard's law, where lattice parameters change linearly with the composition of a dopant, reflecting a well-integrated solid solution. The structural changes in both crystalline size and lattice parameter confirm the successful doping of Cd into the AlCr_2O_4 lattice [22]. The volume of the unit cell for Cd-doped AlCr_2O_4 initially increases with increasing Cd composition, reaching a peak around a composition of 0.04. Beyond this point, the volume remains relatively stable. An initial increase can be attributed to the replacement of smaller Al^{3+} ions (ionic radii 0.53 \AA) with larger Cd^{2+} ions (ionic radii 0.95 \AA) in the AlCr_2O_4 lattice. The larger ionic size of Cd^{2+} leads to lattice expansion, increasing the unit cell volume. The X-ray density decreases steadily as the Cd composition increases. This behaviour is due to the substitution of Al^{3+} ions with Cd^{2+} ions, which have a higher atomic weight but a larger ionic radius. The increase in unit cell volume due to lattice expansion outweighs the increase in mass caused by the addition of heavier Cd ions, leading to an overall decrease in X-ray density (Table-1). The lattice expansion and reduced density can significantly affect the characteristics of the material.

Composition	Crystalline size (nm)	Lattice parameter (\AA)	Volume of unit cell (\AA^3)	X-ray density (g/cm^3)
AlCr_2O_4	23.69	8.225	556.607	4.652
$\text{Al}_{0.96}\text{Cd}_{0.04}\text{Cr}_2\text{O}_4$	25.66	8.755	671.082	3.925
$\text{Al}_{0.9}\text{Cd}_{0.1}\text{Cr}_2\text{O}_4$	23.65	8.767	673.855	4.010

SEM-EDS studies: Fig. 2a-c show the FESEM images of synthesized Cd doped Al nano chromites as the particles appear as aggregated and rod-like structures with rough surfaces. The rods vary in size, with lengths approximately 100 to 200 nm, confirming their nanoscale dimensions. The particles show some degree of agglomeration, which is common in nanomaterials due to the high surface energy. The roughness observed on the particle surfaces suggests a high degree of crystallinity or possible porosity, which may enhance applications such as photocatalysis by increasing the active surface area [23,24].

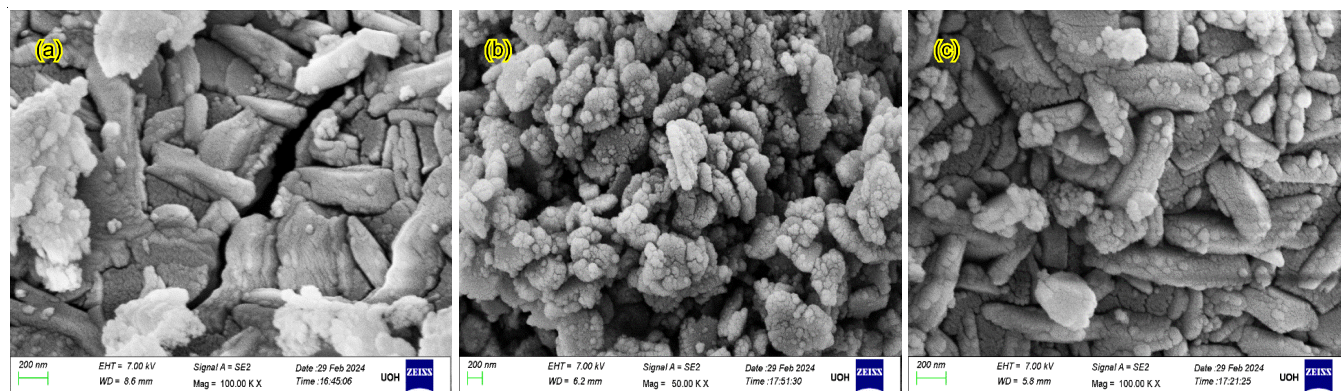


Fig. 2. SEM images of $\text{Al}_{1-x}\text{Cd}_x\text{Cr}_2\text{O}_4$ nanocrystals where $x = 0.00, 0.04$ and 0.10

The energy dispersive spectra of Cd doped Al nano chromites (Fig. 3a-c) confirm the presence of Cd, Al, Cr and O elemental composition of a sample. The spectrum confirms the presence of chromium oxide with possible contributions from cadmium and aluminium.

FTIR studies: FTIR spectra of the prepared Cd doped Al nano chromites provide the insights into their chemical composition, functional groups and molecular interactions. The FTIR spectra of $\text{Al}_{1-x}\text{Cd}_x\text{Cr}_2\text{O}_4$ nanocrystals where $x = 0.00, 0.04$ and 0.10 is shown in Fig. 4a-c. A peak at 600 cm^{-1} corresponds to the stretching vibration of metal-oxygen (M-O) bonds in the tetrahedral sites ($\text{A}^{2+}\text{-O}$). These bonds are shorter and stronger due to the smaller coordination number 4 in the tetrahedral geometry, leading to the higher vibrational frequencies. Whereas the peak at 400 cm^{-1} is associated with the stretching vibration of metal-oxygen bonds in the octahedral sites ($\text{B}^{3+}\text{-O}$) [25]. These bonds are longer and weaker compared to the tetrahedral sites due to the higher coordination number 6, resulting in the lower vibrational frequencies. The distinct positions of these bands help confirm the spinel structure of nanochromites.

Optical studies: Fig. 5 shows the UV-Vis spectra of prepared $\text{Al}_{1-x}\text{Cd}_x\text{Cr}_2\text{O}_4$ where $x = 0.00, 0.04$ and 0.1 with 0.02 variation synthesized by citrate gel auto combustion method recorded from $200\text{-}700 \text{ nm}$ wavelength range [26]. Absorbance of the material decreases as increasing wavelength by analyzing the absorption edge, the optical band gap energy determined, often using Tauc plots [27].

Tauc plots in Fig. 6a-c illustrate the variation in the optical band gap energy (E_g) for AlCr_2O_4 and its Cd-doped Al nano chromites. The undoped AlCr_2O_4 exhibits a band gap of 2.21 eV , indicating its suitability for visible light absorption [28]. The pattern indicates that moderate Cd doping increases the band gap (Table-2), likely due to reduced defect density or structural modifications, while excessive doping reduces it, possibly due to lattice distortion or defect formation [29,30]. Such tunability makes such materials promising for optoelectronic applications.

Photoluminescence studies: Fig. 7a-c shows a broad photoluminescence (PL) emission in the range of $400\text{-}470 \text{ nm}$, peaking near 450 nm suggesting a strong emission in the blue region of visible spectrum. The emission at an excitation wavelength of 350 nm (UV area) indicates the radiative recombination of photoexcited charge carriers. The electronic transitions, invol-

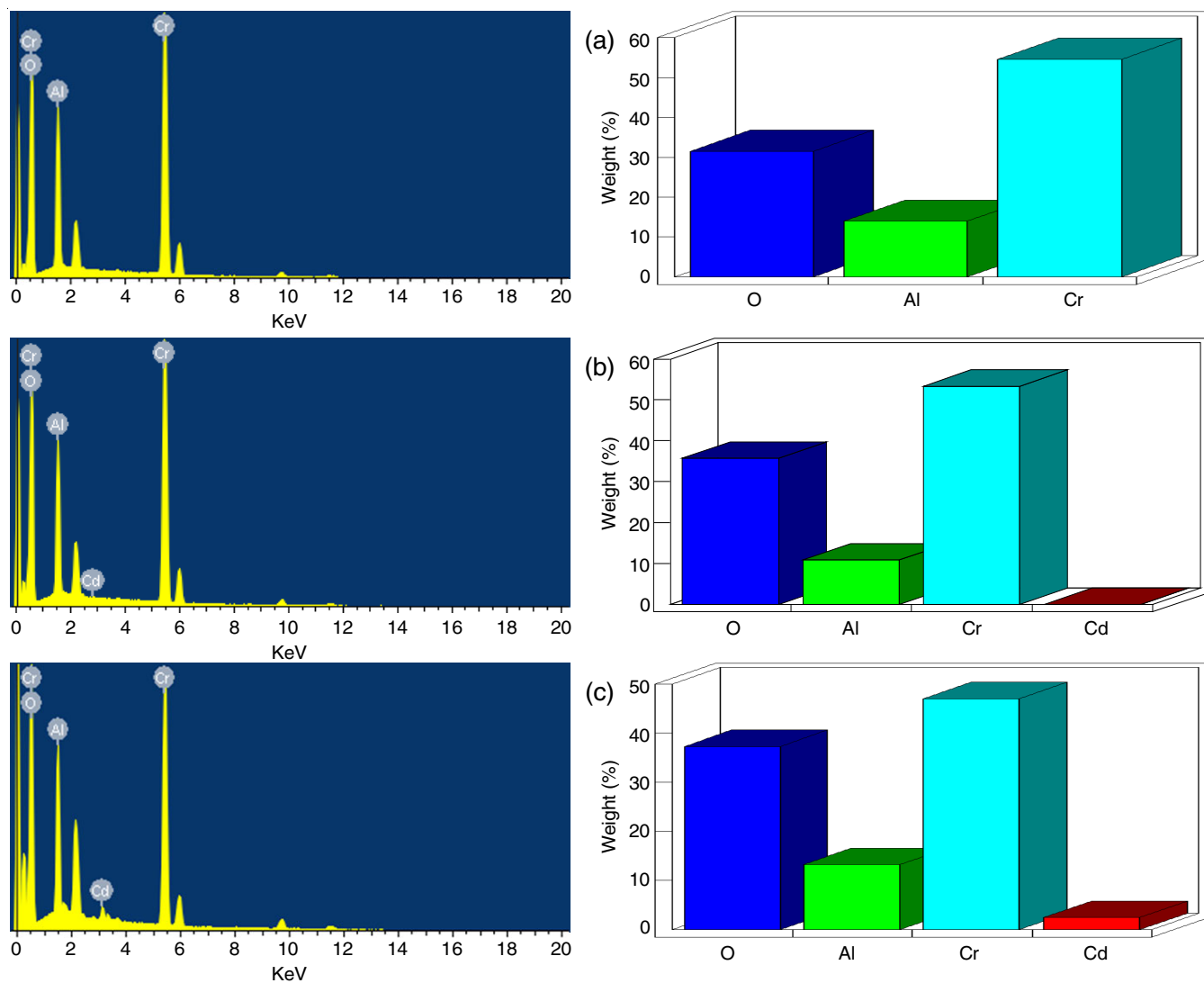


Fig. 3. EDS spectra of $\text{Al}_{1-x}\text{Cd}_x\text{Cr}_2\text{O}_4$ nanocrystals where $x = 0.00, 0.04$ and 0.10

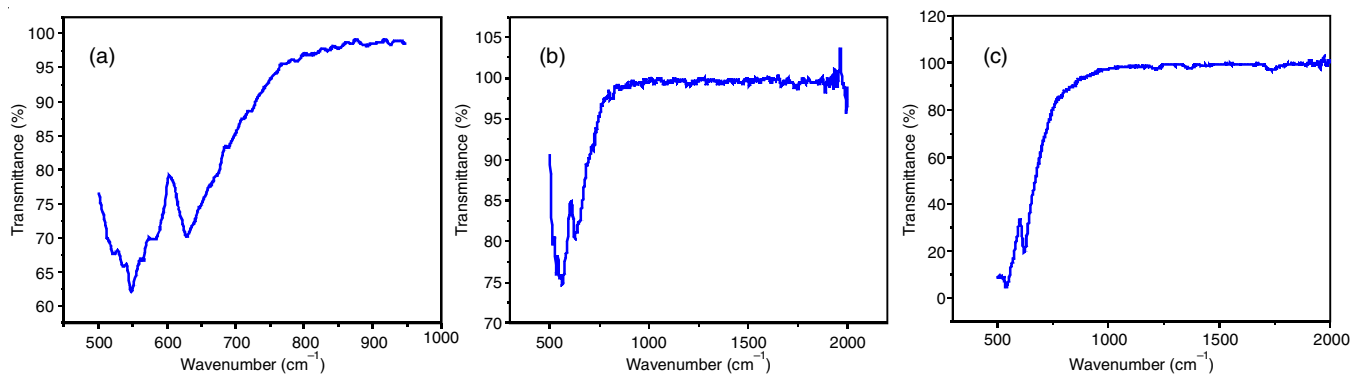


Fig. 4. FTIR spectra of $\text{Al}_{1-x}\text{Cd}_x\text{Cr}_2\text{O}_4$ nanocrystals where $x = 0.00, 0.04$ and 0.10

ving energy levels affected by the aluminum and cadmium dopants, are correlated with the peak at ~ 450 nm. The broadness of the peak indicates the presence of defect states in the material. These may include oxygen vacancies, Cr^{3+} energy levels or dopant induced trap states, which act as intermediate energy levels between the conduction and valence bands [31]. The high PL intensity indicates significant radiative recombination of

electrons and holes, which is favourable for the luminescent applications, it may suggest the limited charge separation and also impact photocatalytic efficiency.

Photocatalytic degradation studies: The photocatalytic activity of methylene blue dye degradation using Al-Cd nanochromites under visible light is depicted in Fig. 8a-c. The absorbance peak of methylene blue detected around 660-670

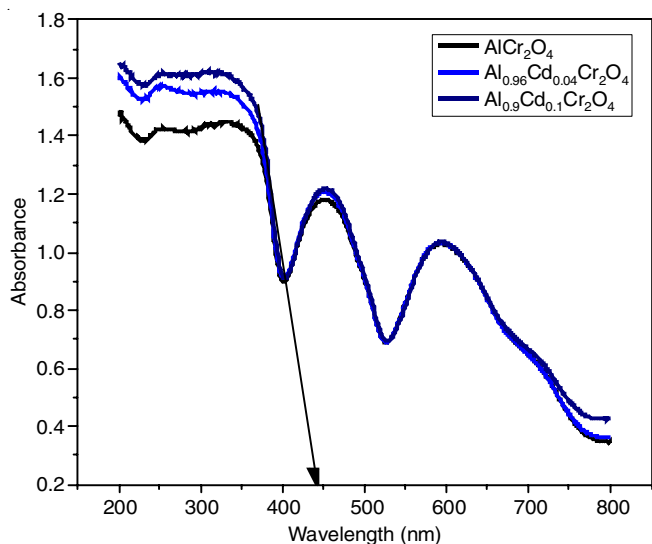


Fig. 5. UV-visible spectra of $Al_{1-x}Cd_xCr_2O_4$ nanocrystals, where $x = 0.00, 0.04$ and 0.10

Cutoff wavelength (nm)	Band gap energy (eV)
440	2.21
424	2.90
440	2.81

nm, progressively decreases as the reaction proceeds, indicating the successful degradation of the dye over time. Initially, at $t = 0$, the absorbance is at its highest, but as visible light activates the Al-Cd nanochromites, the photocatalytic reactions occur,

leading to the breakdown of methylene blue molecules into less harmful byproducts. Significant degradation is observed within the first 45 min, followed by a gradual decline in absorbance up to 90 min, exhibiting the efficient photocatalytic performance of the nano chromites. Fig. 8d demonstrates the photocatalytic degradation of methylene blue using different dosage of catalysts over time. The decrease in C/C_0 indicates the reduction in methylene blue concentration, signifying the photocatalytic activity of the tested materials. In pure and dark conditions, (C/C_0) remains nearly constant, suggesting negligible degradation in the absence of light or catalyst. Among the three tested catalysts, $Al_{0.96}Cd_{0.04}Cr_2O_4$ exhibits the highest photocatalytic efficiency, achieving the greatest reduction in C/C_0 after 75 min [32].

Using Cd doped Al nano chromites, the photocatalytic activity of acid red dye degradation under visible light is shown in Fig. 9a-c. The absorbance peak of acid red at around 530 nm steadily drops as the reaction proceed indicating that acid red dye degraded is successfully over time. Demonstrating the effective photocatalytic function of the nano chromites, significant deterioration was observed within first 45 min, followed by a progressive drop in absorbance up to 90 min.

The photocatalytic degradation of acid red with different composition over time is shown in Fig. 9d. The photocatalytic activity of the studied materials is indicated by the decrease in the C/C_0 , which also shows a decrease in the concentration of methylene blue. Among the three catalysts, $Al_{0.9}Cd_{0.1}Cr_2O_4$ was found to have the highest degradation efficiency, with performance improving quickly from 30 to 90 min. The degradation efficiency depends on the composition of aluminium and cadm-

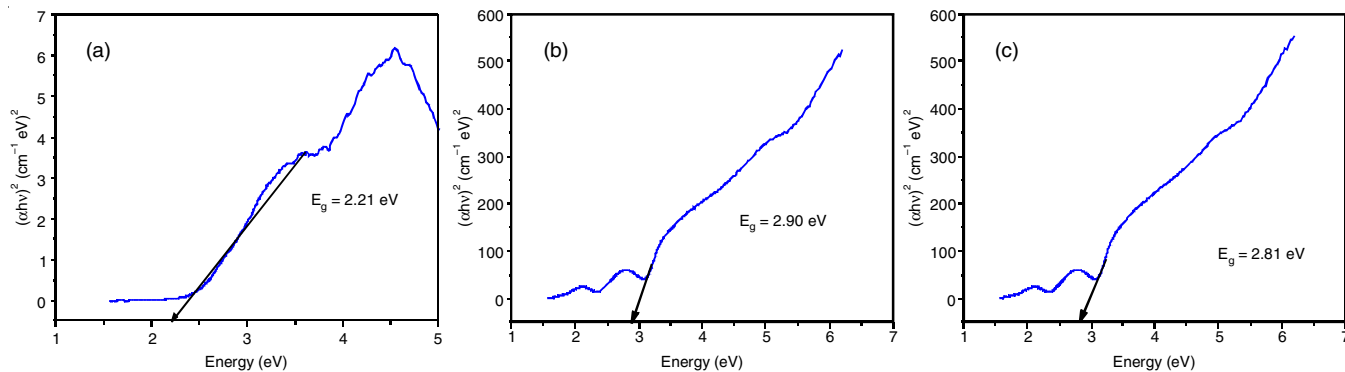


Fig. 6. Tauc plots of $Al_{1-x}Cd_xCr_2O_4$ nanocrystals where $x = 0.00, 0.04$ and 0.10

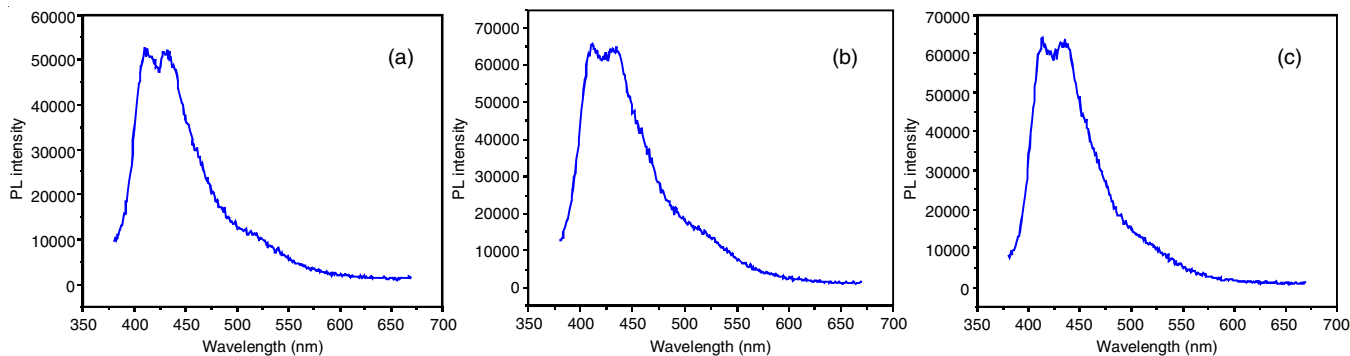


Fig. 7. PL spectra of $Al_{1-x}Cd_xCr_2O_4$ nanocrystals where $x = 0.00, 0.04$ and 0.10

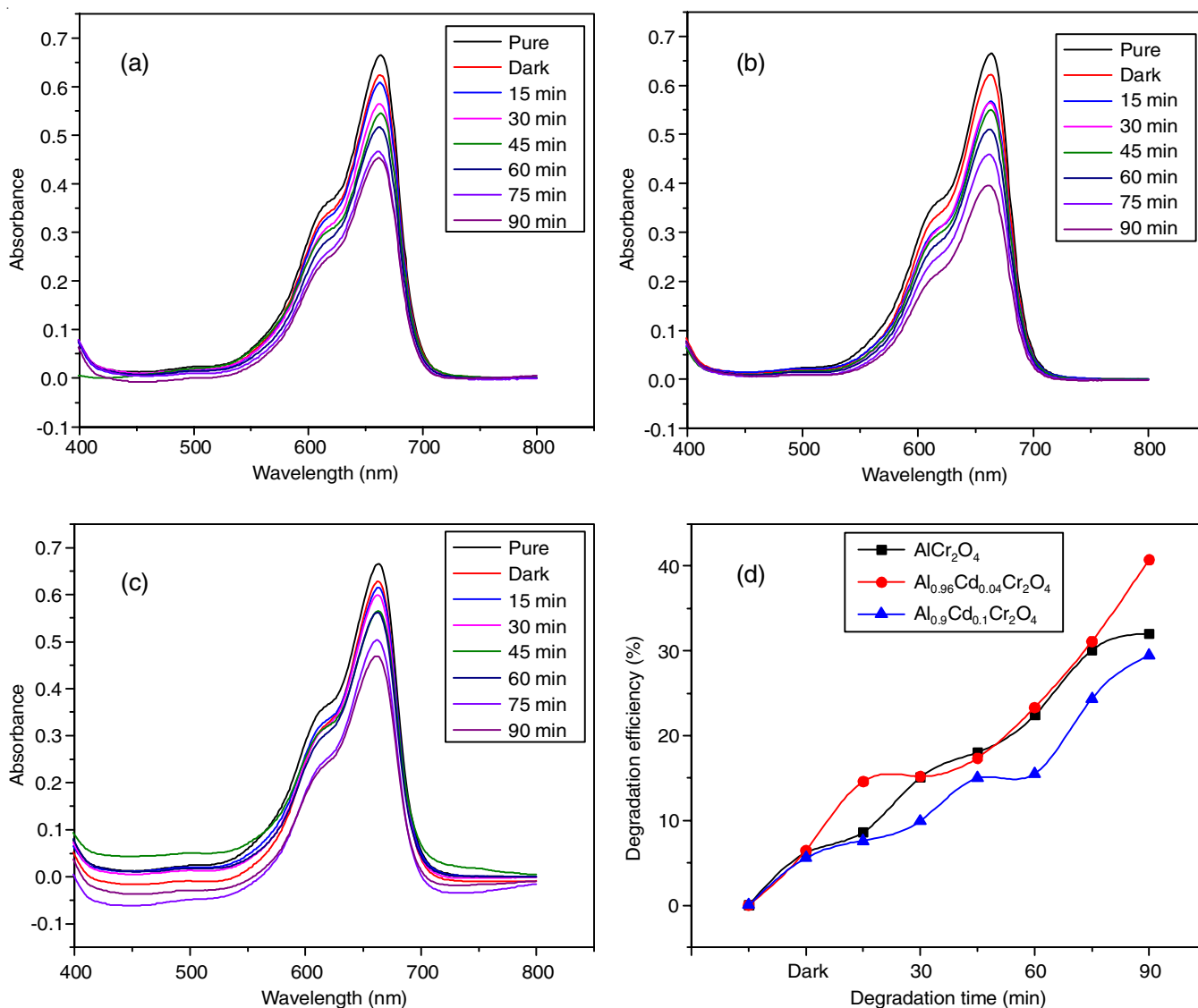


Fig. 8. (a-c) UV-visible absorption spectra of methylene blue of $\text{Al}_{1-x}\text{Cd}_x\text{Cr}_2\text{O}_4$ where $x = 0.00, 0.04$ and 0.10 nano chromites; (d) methylene blue dye degradation against irradiation time of $\text{Al}_{1-x}\text{Ce}_x\text{Cr}_2\text{O}_4$ spinel nano chromates (where $x = 0.00, 0.04$ and 0.10)

ium in the spinel oxide structure. Al-Cr-based oxides generally provide a stable structure, while cadmium enhances photoactivity [32].

Conclusion

The nanostructured cadmium doped Al nano chromites [$\text{Al}_{1-x}\text{Cd}_x\text{Cr}_2\text{O}_4$ where $x = 0.00, 0.04$ and 0.10] were synthesized using the citrate gel auto combustion method at low temperature. XRD spectra revealed that the formation of cubic structure with the space group $Fd\bar{3}m$ and the crystalline sizes range from 23.65 to 25.66 nm. The SEM images revealed the uniform distribution with homogeneity. The FTIR spectra of the samples confirmed the formation of spinel nano chromites as the Cr-O or Al-O stretching vibrations of the tetrahedral sites and the Cd-O octahedral sites appeared at 550 cm^{-1} and 625 cm^{-1} , respectively. The doping of Cd ions to the AlCr_2O_4 matrix causes a structural change resulting in a varying band gap energy values. The peak at 450 nm in the PL spectrum suggests

defect-driven emission in the blue region, indicating successful Cd-Al doping in the chromite samples. It is possible to modify the material's optical characteristics for use in blue-emitting luminous devices. Among the prepared Cd doped Al nano chromites, $\text{Al}_{1-x}\text{Cd}_x\text{Cr}_2\text{O}_4$ with $x = 0.1$ for acid red dye showed the highest dye degradation, but the composition with $x = 0.4$ for methylene blue dye showed the highest degradation.

ACKNOWLEDGEMENTS

The authors are thankful to The Head, Department of Chemistry, Osmania University, Hyderabad, India for providing the necessary facilities to carry out the research work.

CONFLICT OF INTEREST

The authors declare that there is no conflict of interests regarding the publication of this article.

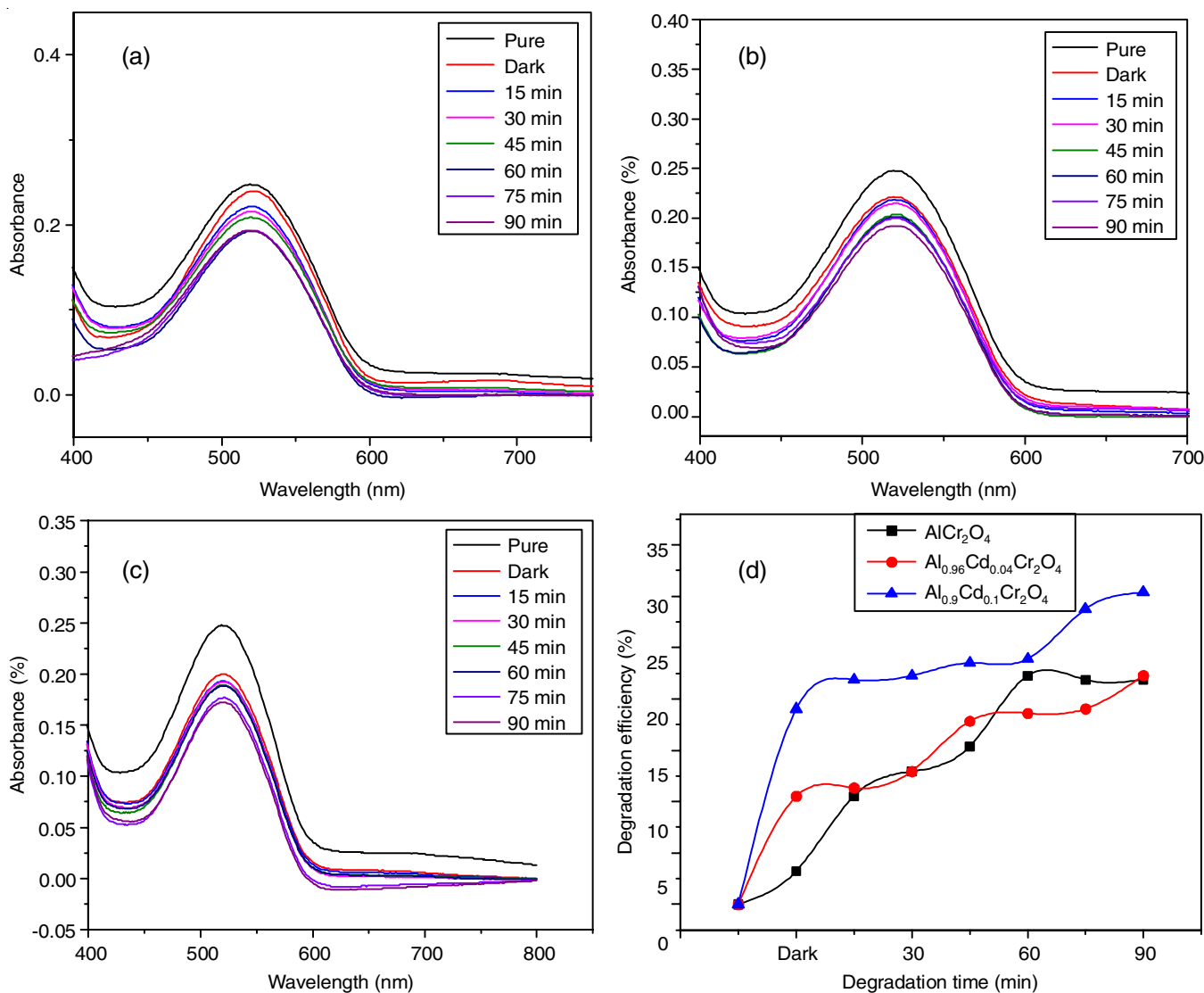


Fig. 9. (a-c) UV-visible absorption spectra of acid red of $\text{Al}_{1-x}\text{Cd}_x\text{Cr}_2\text{O}_4$ where $x = 0.00, 0.04$ and 0.10 nano chromites; (d) acid red dye degradation against irradiation time of $\text{Al}_{1-x}\text{Ce}_x\text{Cr}_2\text{O}_4$ spinel nano chromates (where $x = 0.00, 0.04$ and 0.10)

REFERENCES

- N.R. Mamidipalli, P. Tiyyagura, S. Punna Rao, S.B. Kothamasu, R. Pothu, R. Boddula and N. Al-Qahtani, *Chem. Eng.*, **8**, 100 (2024); <https://doi.org/10.3390/chemengineering8050100>
- M. Priyanka, Y.S. Vidya, H.C. Manjunatha, G.S. Reddy, T.R.K. Reddy, R. Munirathnam, S. Manjunatha, M. Shivanna, E. Krishnakanth and S. Kumar, *Mater. Sci. Eng. B*, **301**, 117190 (2024); <https://doi.org/10.1016/j.mseb.2024.117190>
- Z. Mousavi, M. Esmaeili-Zare and M. Salavati-Niasari, *Trans. Nonferrous Met. Soc. China*, **25**, 3980 (2015); [https://doi.org/10.1016/S1003-6326\(15\)64007-9](https://doi.org/10.1016/S1003-6326(15)64007-9)
- A. Sen and P. Pramanik, *J. Mater. Synth. Process.*, **10**, 107 (2002); <https://doi.org/10.1023/A:1021980211341>
- A.A.H. El-Bassuony and H.K. Abdelsalam, *J. Mater. Sci. Mater. Electron.*, **31**, 3662 (2020); <https://doi.org/10.1007/s10854-020-02924-8>
- Y. Kou, P. Luo, L. Xiao, Y. Xin, G. Zhang, Y. Hu, J. Yang, H. Gao, F. Zhao, W. Jiang and G. Hao, *Defence Technology*, **32**, 120 (2024); <https://doi.org/10.1016/j.dt.2023.04.004>
- P.R. Patil, V.N. Krishnamurthy and S.S. Joshi, *Propellants Explos. Pyrotech.*, **33**, 266 (2008); <https://doi.org/10.1002/prop.200700242>
- M.A. Kassem, A. Abu El-Fadl, A.M. Nashaat and H. Nakamura, *J. Magn. Magn. Mater.*, **495**, 165830 (2020); <https://doi.org/10.1016/j.jmmm.2019.165830>
- F. Paborji, M. Shafiee Afarani, A.M. Arabi and M. Ghahari, *Int. J. Appl. Ceram. Technol.*, **20**, 2203 (2023); <https://doi.org/10.1111/ijac.14376>
- V.T. Vader, *Mater. Res. Bull.*, **85**, 18 (2017); <https://doi.org/10.1016/j.materresbull.2016.08.051>
- M. Ahmadyari-Sharamin and S.A. Hassanzadeh-Tabrizi, *J. Sol-Gel Sci. Technol.*, **99**, 534 (2021); <https://doi.org/10.1007/s10971-021-05590-2>
- S. Naz, S.K. Durrani, M. Mehmood, M. Nadeem and A.A. Khan, *J. Therm. Anal. Calorim.*, **126**, 381 (2016); <https://doi.org/10.1007/s10973-016-5520-9>
- P.S. Kumari, D.R. Kumar, G.V. Charan and S.R. Sagurthi, *Chem. Zvesti.*, **77**, 4727 (2023); <https://doi.org/10.1007/s11696-023-02798-0>
- P. Sailaja Kumari, G. Vijaya Charan and D. Ravi Kumar, *Inorg. Chem. Commun.*, **139**, 109393 (2022); <https://doi.org/10.1016/j.inoche.2022.109393>
- P.O. Oladoye, T.O. Ajiboye, E.O. Omotola and O.J. Oyewola, *Results Eng.*, **16**, 100678 (2022); <https://doi.org/10.1016/j.rineng.2022.100678>

16. National Toxicol Program, *Tech. Rep. Ser.*, **405**, 1 (1991).
17. F. Mohamadpour and A.M. Amani, *RSC Adv.*, **14**, 20609 (2024); <https://doi.org/10.1039/D4RA03259D>
18. Y. El Jabbar, H. Lakhlifi, R. El Ouatib, L. Er-Rakho, S. Guillemet-Fritsch and B. Durand, *Ceram. Int.*, **47**, 9373 (2021); <https://doi.org/10.1016/j.ceramint.2020.12.068>
19. S.M. El-Sheikh and M. Rabbah, *Thermochim. Acta*, **568**, 13 (2013); <https://doi.org/10.1016/j.tca.2013.06.024>
20. S. Naz, S.K. Durrani, M. Mehmood and M. Nadeem, *J. Saudi Chem. Soc.*, **20**, 585 (2016); <https://doi.org/10.1016/j.jscs.2014.12.007>
21. P. Mohanty, C.J. Sheppard, A.R.E. Prinsloo, W.D. Roos, L. Olivi and G. Aquilanti, *J. Magn. Magn. Mater.*, **451**, 20 (2018); <https://doi.org/10.1016/j.jmmm.2017.10.105>
22. X. Xu, J. Gao and W. Hong, *RSC Adv.*, **6**, 29646 (2016); <https://doi.org/10.1039/C5RA27931C>
23. M. Saeed, M. Rani, K. Batool, H. Batool, A. Younus, A. Mehmood, S. Azam, B. Haq, T. Alshahrani, G. Ali and M. Maqbool, *J. Compos. Sci.*, **5**, 247 (2021); <https://doi.org/10.3390/jcs5090247>
24. M. Saeed, M. Rani, K. Batool, H. Batool, A. Younus, A. Mehmood, S. Azam, B. Haq, T. Alshahrani, G. Ali, M. Maqbool, F. Tornabene and T. Triantafillou, *J. Compos. Sci.*, **5**, 247 (2021); <https://doi.org/10.3390/jcs5090247>
25. S.A. Bakar, N. Soltani, W.M.M. Yunus, E. Saion and A. Bahrami, *Solid State Commun.*, **192**, 15 (2014); <https://doi.org/10.1016/j.ssc.2014.05.002>
26. Y. Benrighi, N. Nasrallah, T. Chaabane, H. Belkacemi, K.W. Bourkeb, H. Kenfoud and O. Baaloudj, *J. Sol-Gel Sci. Technol.*, **101**, 390 (2022); <https://doi.org/10.1007/s10971-021-05697-6>
27. V. Mykhailovych, A. Kanak, S. Cojocar, E.-D. Chitoiu-Arsene, M.N. Palamaru, A.-R. Iordan, O. Korovyanko, A. Diaconu, V.G. Ciobanu, G. Caruntu, O. Lushchak, P. Fochuk, Y. Khalavka and A. Rotaru, *Catalysts*, **11**, 1476 (2021); <https://doi.org/10.3390/catal11121476>
28. S. Heni, S. Hcini, M.L. Bouazizi, L. HajTaieb, A. Dhahri and H. Bacha, *RSC Advances*, **14**, 26340 (2024); <https://doi.org/10.1039/D4RA03342F>
29. H. Dhibi, O. Rejaiba, J. Khelifi, M. Nasri, K. Khirouni, M.L. Bouazizi and E.K. Hlil, *J. Inorg. Organomet. Polym. Mater.*, **33**, 3984 (2023); <https://doi.org/10.1007/s10904-023-02703-y>
30. H. Dhibi, O. Rejaiba, J. Khelifi, M. Nasri, O. Amorri, K. Khirouni and M.L. Bouazizi, *J. Sol-Gel Sci. Technol.*, **108**, 159 (2023); <https://doi.org/10.1007/s10971-023-06178-8>
31. S. Taghavi Fardood, R. Forootan, F. Moradnia, Z. Afshari and A. Ramazani, *Mater. Res. Express*, **7**, 015086 (2020); <https://doi.org/10.1088/2053-1591/ab6c8d>
32. M. Khatamian, E. Dastar, S. Fazli-Shokouhi and S. Hosseini Nami, *J. Indian Chem. Soc.*, **20**, 2805 (2023); <https://doi.org/10.1007/s13738-023-02877-9>